

## Near-infrared light-driven asymmetric photolytic reduction of ketone using inorganic-enzyme hybrid biocatalyst

Qiao, Li; Zhang, Jing; Jiang, Yongjian; Ma, Bianqin; Chen, Haomin; Gao, Peng; Zhang, Pengfei; Wang, Anming; Sheldon, Roger A.

**DOI**

[10.1016/j.ijbiomac.2024.130612](https://doi.org/10.1016/j.ijbiomac.2024.130612)

**Publication date**

2024

**Document Version**

Final published version

**Published in**

International Journal of Biological Macromolecules

**Citation (APA)**

Qiao, L., Zhang, J., Jiang, Y., Ma, B., Chen, H., Gao, P., Zhang, P., Wang, A., & Sheldon, R. A. (2024). Near-infrared light-driven asymmetric photolytic reduction of ketone using inorganic-enzyme hybrid biocatalyst. *International Journal of Biological Macromolecules*, 264, Article 130612. <https://doi.org/10.1016/j.ijbiomac.2024.130612>

**Important note**

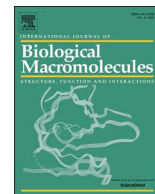
To cite this publication, please use the final published version (if applicable). Please check the document version above.

**Copyright**

Other than for strictly personal use, it is not permitted to download, forward or distribute the text or part of it, without the consent of the author(s) and/or copyright holder(s), unless the work is under an open content license such as Creative Commons.

**Takedown policy**

Please contact us and provide details if you believe this document breaches copyrights. We will remove access to the work immediately and investigate your claim.



# Near-infrared light-driven asymmetric photolytic reduction of ketone using inorganic-enzyme hybrid biocatalyst

Li Qiao<sup>a</sup>, Jing Zhang<sup>a</sup>, Yongjian Jiang<sup>a</sup>, Bianqin Ma<sup>a</sup>, Haomin Chen<sup>a</sup>, Peng Gao<sup>a,\*</sup>, Pengfei Zhang<sup>a</sup>, Anming Wang<sup>a,\*</sup>, Roger A. Sheldon<sup>b,c,\*\*</sup>

<sup>a</sup> Key Laboratory of Organosilicon Chemistry and Materials Technology, Ministry of Education, College of Materials Chemistry and Chemical Engineering, Hangzhou Normal University, Hangzhou 311121, Zhejiang, China

<sup>b</sup> Molecular Sciences Institute, School of Chemistry, University of the Witwatersrand, PO Wits, 2050 Johannesburg, South Africa

<sup>c</sup> Department of Biotechnology, Section BOC, Delft University of Technology, Van der Maasweg 9, 2629 HZ Delft, the Netherlands

## ARTICLE INFO

### Keywords:

Photo-enzymatic reduction  
Cofactor regeneration  
Upconversion  
TiO<sub>2</sub>/r-GQDs nanocomposite  
Aldo-ketone reductase  
Ketone reduction

## ABSTRACT

Effective photolytic regeneration of the NAD(P)H cofactor in enzymatic reductions is an important and elusive goal in biocatalysis. It can, in principle, be achieved using a near-infrared light (NIR) driven artificial photosynthesis system employing H<sub>2</sub>O as the sacrificial reductant. To this end we utilized TiO<sub>2</sub>/reduced graphene quantum dots (r-GQDs), combined with a novel rhodium electron mediator, to continuously supply NADPH in situ for aldo-keto reductase (AKR) mediated asymmetric reductions under NIR irradiation. This upconversion system, in which the Ti-O-C bonds formed between r-GQDs and TiO<sub>2</sub> enabled efficient interfacial charge transfer, was able to regenerate NADPH efficiently in 64 % yield in 105 min. Based on this, the pharmaceutical intermediate (R)-1-(3,5-bis(trifluoromethyl)phenyl)ethan-1-ol was obtained, in 84 % yield and 99.98 % ee, by reduction of the corresponding ketone. The photo-enzymatic system is recyclable with a polymeric electron mediator, which maintained 66 % of its original catalytic efficiency and excellent enantioselectivity (99.9 % ee) after 6 cycles.

## 1. Introduction

Enzymatic asymmetric reductions with AKRs, a class of ketone reductases (KREDs), are a valuable method for synthesizing high-value chiral chemicals in the pharmaceuticals, pesticide and perfume industries [1,2]. They are highly efficient, exhibit excellent enantioselectivities and have a wide substrate specificity range [3–5]. However, the expensive nicotinamide adenine dinucleotide [NAD(P)H] cofactor is required in stoichiometric amounts for these biotransformations [6]. This is usually achieved by using a second, sacrificial substrate and/or a second enzyme. In principle, photocatalysis offers a sustainable alternative by exploiting a light-harvesting system and electron transport chains to drive the biocatalytic conversion of inexhaustible green solar energy into chemical energy for cofactor regeneration [7–9].

Photosensitizers ranging from organic dyes [10–12] (e.g., porphyrins, xanthenes, ruthenium complexes, flavins), semiconducting materials [13,14] (e.g., quantum dots, carbon nitrides, TiO<sub>2</sub>), to diverse hybrid materials [15,16] have been intensively studied for light-driven

redox biosynthesis. However, the weak penetration ability of ultraviolet or visible light in various reaction media is a serious problem because the components of biological tissues, including proteins, nucleic acids, phospholipids, and other various sized molecules, absorb visible light much more strongly than chemical reaction media do [17]. Although infrared (IR) light [18] contains half of the energy of sunlight and has considerable penetration depth in complex systems such as biological tissues, its photon energy is relatively low and usually not sufficient to directly stimulate photocatalysts in photochemical reactions.

Upconversion is a non-linear optical phenomenon whereby low energy photons stimulate the emission of higher-energy photons [19]. Upconversion nanomaterials are widely applied in bio-imaging, solar cells, optical biosensors and nonlinear optical properties [20,21]. They can indirectly broaden the absorption ranges of semiconductors by turning the captured long-band incident light into shorter-band visible or ultraviolet light [22]. Various NIR-light-active photocatalysts, based on rare earth-doped upconverting particles (UCPs) [23,24], quantum dots [25,26], defective materials [27], complicated heterostructures

\* Corresponding authors.

\*\* Correspondence to: R.A. Sheldon, Molecular Sciences Institute, School of Chemistry, University of the Witwatersrand, PO Wits, 2050 Johannesburg, South Africa.  
E-mail addresses: [waming@hznu.edu.cn](mailto:waming@hznu.edu.cn) (A. Wang), [roger.sheldon@wits.ac.za](mailto:roger.sheldon@wits.ac.za), [r.a.sheldon@tudelft.nl](mailto:r.a.sheldon@tudelft.nl) (R.A. Sheldon).

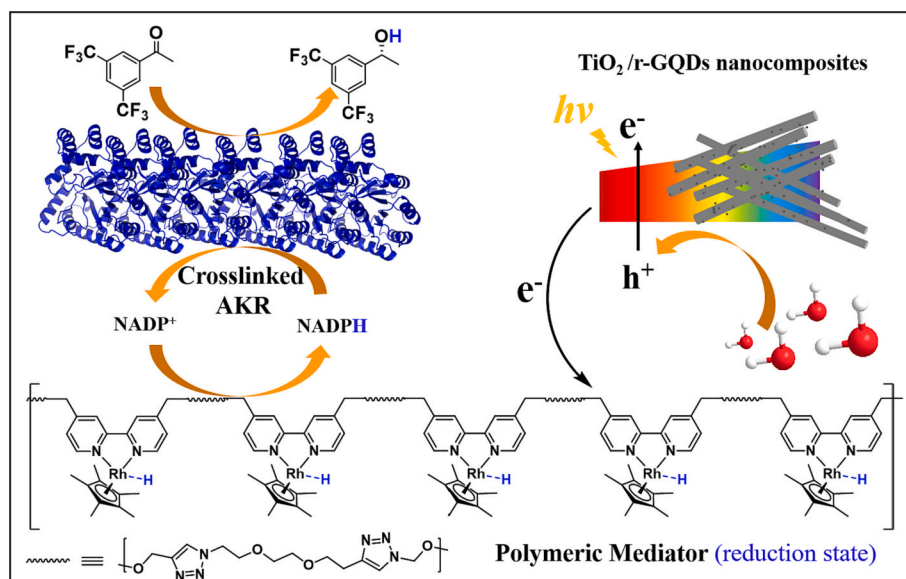


Fig. 1. Schematic illustration of the NIR-mediated photo-enzymatic reduction of ketone.

[28,29], and organic triplet–triplet annihilation upconversion materials [30] were used. Nevertheless, building an effective photo-enzymatic catalysis system remains a huge challenge given the biocompatibility and photostability of each component [31–33]. Previously, Park et al. employed silica-coated UCs, Si-NaYF<sub>4</sub>:Yb,Er with rose bengal for NIR-light-driven NADH regeneration and photoenzymatic synthesis of L-glutamate but the overall catalytic efficiency was low [34].

Inorganic TiO<sub>2</sub> and quantum dots are both widely applied semiconductor materials with high chemical stability, non-toxicity and low cost [35–37]. Recently, inspired by our discovery that hybrid materials based on TiO<sub>2</sub>/reduced graphene quantum dots (r-GQDs) promote interfacial multiphoton-generated electron transfer via Ti-O-C linkages, we found that they have strong infrared light photocatalytic activity for water splitting and CO<sub>2</sub> reduction [38,39]. Hence, we envisioned that TiO<sub>2</sub>/r-GQD composites could be adapted to address the long excitation wavelength challenges of cofactor regeneration in a photo-enzymatic cascade system.

Enzyme immobilization can be used [40] to enhance the stability of the free enzymes, e.g. towards ligand exchange with metal complexes [41,42]. For example, the insertion of non-canonical amino acids (ncAAs) [43–45], bearing bioorthogonal groups at appropriate sites, provides a suitable method for generating self-cross-linked enzymes with complete retention of activity. Consequently, we prepared novel upconversion nanocomposites consisting of TiO<sub>2</sub> nanotubes and reduced graphene quantum dots. The TiO<sub>2</sub>/r-GQDs nanotubes enabled the utilization of near-infrared light to transfer electrons to a rhodium complex, thereby affording a sunlight-activated photocatalytic system for cofactor regeneration. Subsequent combination with the AKR assembly exhibited good biocompatibility and recyclability in the asymmetric photo-enzymatic reduction of ketones to valuable chiral alcohol enantiomers (Fig. 1). This forms the basis for a green and sustainable infrared light-driven photo-enzymatic system.

## 2. Materials and methods

### 2.1. Materials

Rhodium(III) trichloride hydrate (RhCl<sub>3</sub>·3H<sub>2</sub>O, 98 %), ethylenediaminetetraacetic acid (EDTA, 99 %), sodium hydride (NaH, 60 %), 2,2'-bipyridine-4,4'-dimethanol (98 %), 3,5-bis(trifluoromethyl)acetophenone (3,5-BTAP, 98 %), 3-bromopropyne (propargyl bromide, 98 %) and 1,2,3,4,5-pentamethylcyclopentadiene (95 %) were purchased

from Shanghai Aladdin Bio-Chem Technology Co., Ltd., Shanghai, China. Dibenzocycloocta-4a,6a-diene-5,11-diyne (DBA, 99 %), sodium chloride (NaCl, AR), hydrochloric acid (HCl, 37 %), β-nicotinamide adenine dinucleotide sodium salt (NADP<sup>+</sup>, 95 %), dichloromethane (CH<sub>2</sub>Cl<sub>2</sub>, AR), sodium sulfate (Na<sub>2</sub>SO<sub>4</sub>, AR) and methyl alcohol (MeOH, AR) originated from Senrise Bio-Chem Technology Co., Ltd., Shanghai, China.

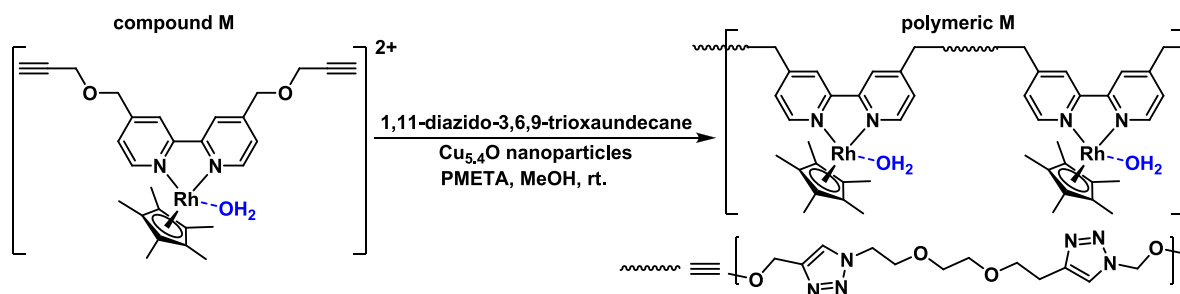
### 2.2. Microwave-assisted covalent assembly of AKR two-point variants

AKR assembly rings were prepared according to the published methods [46]. To a solution of the AKR two-point mutants in pH 7.0 PBS (0.02 mol·L<sup>-1</sup>) was added 1.0 mL isopropanol solution containing the cross-linker DBA (8 mmol·L<sup>-1</sup>). The molar ratio of azide groups and alkyne groups in the reaction was 2:1. The mixture was placed in a microwave reactor equipped with a cooling module and a continuously illuminated device, and irradiated for three minutes (Discover Cool-Mate, CEM, USA). Then the cross-linked enzyme was separated and washed with 2 M NaCl solution and deionized water until no protein was detected in the supernatant. Enzymes remaining in the supernatant were determined by Bradford analysis. The morphology and dimensions of the enzyme-protein assemblies were characterized by SEM and CLSM.

### 2.3. Synthesis and characterization of the mediator

#### 2.3.1. Synthesis of 4,4'-bis(prop-2-yn-1-yloxy) methyl-2,2'-bipyridine

To a mixture of 2,2'-bipyridine-4,4'-dimethanol (500 mg, 2.3 mmol) and NaH (276 mg, 11.5 mmol) in dry DMF (10 mL) was added propargyl bromide (595 μL, 6.9 mmol) under N<sub>2</sub> atmosphere. The reaction mixture was stirred at room temperature for 4 h until TLC (hexane-EtOAc; 2:1) showed complete conversion of the starting material. After the reaction, MeOH was carefully added to neutralize the excess NaH and the solvent was evaporated in vacuo. The residue was dissolved in CH<sub>2</sub>Cl<sub>2</sub> (20 mL) and washed successively with H<sub>2</sub>O (20 mL) and brine (20 mL). Subsequently, organic layers were dried over anhydrous Na<sub>2</sub>SO<sub>4</sub> and concentrated under reduced pressure. The crude product (Fig. S2A, compound 1) was purified by flash chromatography using hexane/EtOAc (3,1) as eluent to obtain pure compounds, which were characterized by NMR and mass spectrometry (Fig. S1). Obtained as a white solid, 103.6–105.2 °C. <sup>1</sup>H NMR (CDCl<sub>3</sub>, 500 MHz) δ 8.51–7.35 (m, 6H, ArH), 4.72 (s, 4H, CH<sub>2</sub>C=CH), 4.27 (d, 4H, J = 2.4 Hz, CH<sub>2</sub>OCH<sub>2</sub>C=CH), 2.49 (t, 2H, J = 2.4 Hz, C=CH). <sup>13</sup>C NMR (126 MHz, CDCl<sub>3</sub>) δ 156.0,



Scheme 1. The polymerization reaction of  $[\text{Cp}^*\text{Rh}(\text{bipy})(\text{H}_2\text{O})]^{2+}$  with cross-linker.

149.3, 147.9, 122.1, 119.5, 79.1, 75.2, 70.0, 57.9, 25.6.

### 2.3.2. Synthesis of $[\text{Cp}^*\text{Rh}(\text{bipy})(\text{H}_2\text{O})]^{2+}$

The electron mediator  $[\text{Cp}^*\text{Rh}(\text{bipy})(\text{H}_2\text{O})]^{2+}$  was synthesized using a published procedure [47]. Initially, a solution of  $\text{RhCl}_3 \cdot 3\text{H}_2\text{O}$  and 1,2,3,4,5-pentamethylcyclopentadiene (1.0 equiv.) in methanol was refluxed for 15 h to form a red precipitate of  $[\text{Cp}^*\text{RhCl}_2]$ . The latter was filtered and then suspended in methanol. The addition of 2.0 equiv. of 4,4'-bis((prop-2-yn-1-yloxy)methyl)-2,2'-bipyridine caused a colour change to light yellow. The desired metal complex  $[\text{Cp}^*\text{Rh}(\text{bipy})(\text{H}_2\text{O})]^{2+}$  was precipitated by the addition of ether for the hydrolysis of  $[\text{Cp}^*\text{Rh}(\text{bipy})\text{Cl}]\cdot\text{Cl}$ . The light brown Rh(III) complex stock solution (100 mM) was prepared in water, stored at room temperature, and characterized analytically by LC-MS (Fig. S2B). According to the mass spectrometry results, the corresponding peak  $[\text{M}_{\text{C}29\text{H}35\text{N}2\text{O}2\text{RhCl}+\text{Na}}]^+$  was found for 604.1352 (Fig. S2).

### 2.3.3. Synthesis of $[\text{Cp}^*\text{Rh}(\text{bipy})(\text{H}_2\text{O})]^{2+}$ polymers

As Scheme 1, to a mixture of  $[\text{Cp}^*\text{Rh}(\text{bipy})\text{Cl}]\cdot\text{Cl}$  (0.1 mM), 1,11-diazido-3,6,9-trioxaundecane cross-linker (0.06 mM), pentamethyldiethylenetriamine (PMETA, 0.1 mM) and MeOH (1 mL) was added 1 mL  $\text{Cu}_{5,4}\text{O}$  nanoparticles solution [48] under air atmosphere for 12 h. The formation of  $[\text{Cp}^*\text{Rh}(\text{bipy})]^{2+}$  polymers was based on a click chemistry reaction [49]. The crude product was precipitated by the addition of anhydrous ether, then was separated and washed with saturated EDTA solution, deionized water and MeOH successively to afford dark brown  $[\text{Cp}^*\text{Rh}(\text{bipy})(\text{H}_2\text{O})]^{2+}$  polymers.

## 2.4. Synthesis of the photocatalyst

### 2.4.1. Preparation of r-GQDs

Glucose was dispersed in 40 mL of pure water and stirred with a magnetic stirrer for 10 min. The mixture was heated at 190 °C for 3 h in a Teflon-lined autoclave. After cooling to room temperature, the resulting brown solution was centrifuged for 20 min to remove the precipitate and retain GQDs dispersed in the supernatant. 50 mg  $\text{NaBH}_4$  was added to the aqueous suspension of GQDs (0.1–1  $\text{mg}\cdot\text{mL}^{-1}$ ) and the mixture was stirred at room temperature for 4 h to afford r-GQDs.

### 2.4.2. Preparation of $\text{TiO}_2$ nanotubes

1 g  $\text{TiO}_2$  nanopowder was dispersed in 100 mL of 10 M NaOH and stirred in a beaker for 30 min. The mixture was then placed in a Teflon-lined autoclave at 140 °C for 18 h. After the autoclave had naturally cooled to room temperature, the resulting precipitate was recovered by filtration and washed with deionized water and 0.1 M HCl solution for 6 h. Subsequently, the solid was washed 2–3 times until the pH reached 7.0, dried at 80 °C for 24 h and then calcined in air at 400 °C for 2 h to afford the desired  $\text{TiO}_2$  nanotubes.

$\text{TiO}_2/\text{r-GQDs}$  composites were obtained by adding 0.2 g  $\text{TiO}_2$  to a 40 mL r-GQDs suspension and continuously stirring at room temperature for 4 h to obtain a homogeneous suspension. The  $\text{TiO}_2/\text{r-GQDs}$  were collected by centrifugation, washed 3 times with distilled water, and

dried under vacuum at 60 °C overnight.

## 2.5. Regeneration of NADPH under NIR excitation

The photochemical reaction medium for NADPH regeneration consisted of PBS buffer (pH 7.0, 200 mM, 25 mL),  $\text{NADP}^+$  (0.05 mM, 93 mg) and 0.25 mM  $[\text{Cp}^*\text{Rh}(\text{bipy})(\text{H}_2\text{O})]^{2+}$  or  $[\text{Cp}^*\text{Rh}(\text{bipy})(\text{H}_2\text{O})]^{2+}$  polymers. After the addition of photocatalyst  $\text{TiO}_2/\text{r-GQDs}$  (20 mg) and ultrasonic dispersion for 10 min, the photoreduction of  $\text{NADP}^+$  was performed at room temperature by irradiation with NIR (800 nm–1100 nm). The distance between the reactor and light source (Xe lamp with an optical filter, 300 W) was fixed at 15 cm to provide approximately 20  $\text{mW}\cdot\text{cm}^{-2}$  illumination intensity. The produced cofactor was determined at different reaction times by UV absorption (Beckman DU-800 UV spectrophotometer) at 340 nm. For the reusability test,  $\text{TiO}_2/\text{r-GQDs}$  and M polymers were rigorously washed with deionized water, and collected by centrifugation.

## 2.6. Photo-enzymatic production of (R)-3,5-BTPE

In a typical procedure for photo-enzymatic synthesis of (R)-3,5-BTPE, the entire 5 mL system consisted of PBS buffer (200 mM, 4.5 mL, pH 7.0),  $\text{NADP}^+$  (1 mM, 37.2 mg), 0.25 mM  $[\text{Cp}^*\text{Rh}(\text{bipy})(\text{H}_2\text{O})]^{2+}$ , 4 mg  $\text{TiO}_2/\text{r-GQDs}$ , 2 mg enzyme assemblies, and 3 mg substrate 3,5-bis(trifluoromethyl)acetophenone (3,5-BTAP) at a final concentration of 6.25 mM. The solution was placed in a quartz reactor with a small stirrer and irradiated for 18 h. To avoid damage to the enzyme from increasing temperature, the xenon lamp was placed about 15 cm from the reactor. The product was extracted from the supernatant and analyzed by chiral HPLC (Agilent 1100) to determine the ratio of isomers. Analyses were performed using a DaicelIC column (4.6 × 250 mm, 5  $\mu\text{m}$  particle size) at a column temperature of 30 °C. The mobile phase was methanol and water (75:25 v/v) with a flow rate of 0.5 mL/min. The injection volume was 10  $\mu\text{L}$ . The purified substrate and reduced product were used as standard samples to verify the retention time, and data were collected at 210 nm. For every reuse of the hybrid catalyst, the reaction was performed for 10 h.  $\text{TiO}_2/\text{r-GQDs}$ , AKR assembly and polymeric M were recycled by centrifugal separation from the reaction mixture.

## 3. Results and discussion

### 3.1. Covalent assemblies of AKR

Aldo-keto reductase (AKR, Gene ID: 897867) catalyses the asymmetric reduction of aromatic ketones to the corresponding chiral alcohols. Since the cyclic enzyme assemblies showed enhanced enzymatic activity and high robustness in terms of stability towards acidity and temperature, we expect them to enable long-lasting catalysis in the photo-biocatalytic synthesis of chiral alcohols. The preparation of AKR ring assemblies has been described in our previous studies [46]. With the two *p*-azido-*L*-phenylalanine (*p*-AzF) residues inserted into the 114Y and 189Q of the AKR protein using the protein engineering technique,

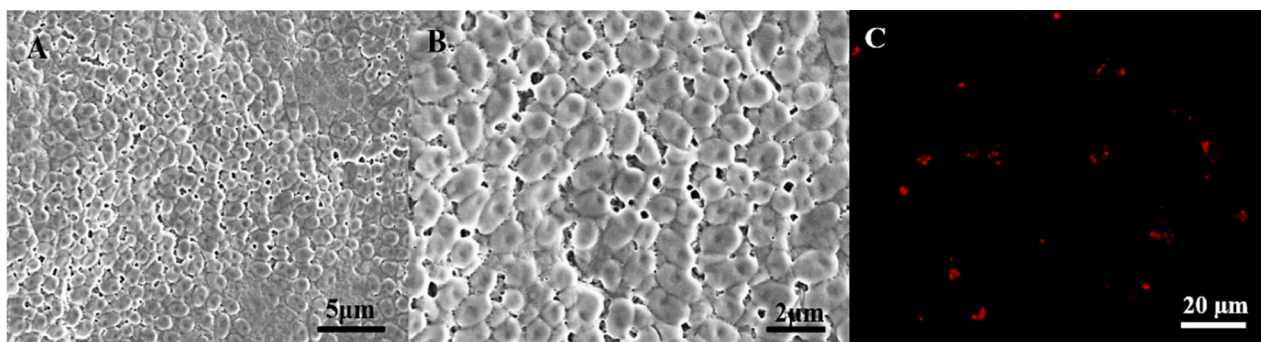


Fig. 2. SEM (A, B) and CLSM (C) images of AKR assemblies.

we cross-linked the AKR-114-189 mutant with the cross-linker DBA via microwave-assisted strain-promoted azide-alkyne cycloaddition. The morphologies of resulting ring assemblies were characterized by scanning electron microscopy (SEM). As shown in Fig. 2, the approximate size of AKR assemblies is 1–2  $\mu\text{m}$ . We then stained them by using Sulfo-Cyanine5 (CY5), which was specifically bonded to the 6xHis tag in monomer protein. Under 640 nm exciting light, the independent, cross-linked AKR were visualized in red by laser scanning microscope (CLSM) and exhibited an unformed aggregation state (Fig. 2C).

### 3.2. Characterization of electron transfer mediators and upconversion photocatalyst

The organometallic complex, pentamethylcyclopentadienyl rhodium 2,2'-bipyridine ( $[\text{Cp}^*\text{Rh}(\text{bpy})\text{H}_2\text{O}]^{2+}$ ), is the most studied electron mediator and hydride transfer agent used in photochemical regeneration of 1,4-NAD(P)H [50,51]. To explore the sustainability of the designed photo-biocatalytic system, we devised polymeric Rh(III) complexes to enable the recycling of key components and the recovery of precious metal rhodium materials. Two alkyne moieties were introduced into the bipyridine ligand of  $[\text{Cp}^*\text{Rh}(\text{bipy})\text{H}_2\text{O}]^{2+}$  (**M**). Subsequently,  $[\text{Cp}^*\text{Rh}(\text{bipy})\text{H}_2\text{O}]^{2+}$  polymers were produced by copper nanoparticle catalysed alkyne-azide cycloaddition reaction with a cross-linking agent containing two azide groups. The macromolecular Rh(III) complex formed by aggregation, could be separated from reaction solutions conveniently by centrifugal sedimentation.

The bipyridine ligand was aggregated as a control. The SEM images of the polymeric ligand and Rh (III) mediator (**M**) reveal that both of the polymers are amorphous (Fig. 3A, C). The polymeric ligand consists of three elements: C, N, and O (Fig. 3B). As expected, the energy-dispersive X-ray spectroscopy (EDS) mapping of polymeric **M** shows C, N, O, Rh, Cl homogeneously dispersed over the whole structure with no copper residues (Fig. 3D, E). The stepwise preparation of the polymeric mediator was followed using Fourier transform infrared spectroscopy (FT-IR) by noting prominent changes in the frequency pattern of functional groups (Fig. 4A1). Substitution of alkyne groups at the para position of the bipyridine ligand produced two strong characteristic peaks at 3173  $\text{cm}^{-1}$  and 2102  $\text{cm}^{-1}$ , which are assigned to the typical stretching modes of  $\equiv\text{C-H}$  and  $\text{C}\equiv\text{C}$  bond, respectively. For **M**, the  $\nu_{\text{C-H}}$  has a red shift and was overlapped by the broad peak (3386–3246  $\text{cm}^{-1}$ ), which is a significant marker for distinguishing the metal complex from its ligand, indicating the successful coordination of rhodium ions. The disappearance of  $\nu_{\text{C}\equiv\text{C}}$  in polymeric **M** reveals the effectiveness of the cross-linking strategy used. The coordinated Rh is also validated by the presence of Rh 3d peak in the XPS spectra of polymeric **M**. The peaks appearing at 314.0 eV and 309.0 eV are assigned to the binding energies of Rh 3d<sub>2/3</sub> and Rh 3d<sub>5/2</sub>, respectively (Fig. 4A2) [52,53]. In addition, the multi-cross-linked bipyridine ligand was detected by Matrix-assisted laser desorption/ionization (Fig. S3).

The target  $\text{TiO}_2/\text{r-GQD}$  nano photocatalyst was synthesized using an

impregnation strategy. The morphology and microstructure of the synthesized photocatalytic materials were examined by SEM (Fig. 4B1). The  $\text{TiO}_2/\text{r-GQDs}$  composites are mainly tubular and arranged in a disordered manner with a length of a few hundred nanometres and a width of about 20 nm to about 40 nm. In comparison with the standard powder X-ray diffraction (XRD) spectra of  $\text{TiO}_2$  [38], the diffraction peaks of  $\text{TiO}_2/\text{r-GQDs}$  at (116), (220), and (215) crystal planes are significantly depressed, indicating the successful coupling of r-GQDs and  $\text{TiO}_2$  (Fig. 4B2). According to FT-IR investigation, the oxygen-containing OH groups ( $\sim 3400 \text{ cm}^{-1}$ ) in  $\text{TiO}_2/\text{r-GQDs}$  are significantly reduced compared to that of  $\text{TiO}_2$  alone, mainly due to the coverage of quantum dots (Fig. S4A). Moreover, r-GQDs with a large number of dangling bonds of carbon would combine with the oxygen atoms on the  $\text{TiO}_2$  surface to generate Ti-O-C chemical bonds, which is consistent with the peaks observed at 950  $\text{cm}^{-1}$  of  $\text{TiO}_2/\text{r-GQDs}$  FT-IR line [54,55]. The formation of these Ti-O-C chemical bonds was further confirmed using X-ray photoelectron spectroscopy (XPS). The  $\text{TiO}_2/\text{r-GQD}$  composites show the presence of O, Ti and C elements (Fig. 4B3), consistent with r-GQDs on  $\text{TiO}_2$  NTs, and exhibited the typical peaks for Ti-O-C bonds at 288.4 eV, 531.6 eV and 457.8 eV, which are assigned to C 1s, O 1s and Ti 2p (Fig. S4B-D) of XPS spectra, respectively.

The charge dynamics were studied by Photoluminescence (PL) Spectroscopy. As shown in Fig. 4B4, the multiphoton emission of r-GQDs induced by upconversion was detected at 522 nm, 542 nm, and 654 nm under infrared light excitation at 980 nm. The multiphoton active process testifies to the competence of  $\text{TiO}_2/\text{r-GQDs}$  nanotubes for acting as a powerful energy transfer component.

### 3.3. Regeneration of NADPH by photoredox catalysis

Photocatalytic water decomposition for NADPH regeneration over  $\text{TiO}_2/\text{r-GQDs}$  nano-composite is a zero-carbon scheme. The anticipated results would contribute strongly to the ‘‘Sustainable Development Goals’’, and not generate carbon-containing and difficult-to-separate by-products during or after the regeneration process. By design, we performed the photochemical reduction assays of  $\text{NADP}^+$  in PBS buffer using  $\text{TiO}_2/\text{r-GQDs}$  nanotubes and  $[\text{Cp}^*\text{Rh}(\text{bipy})(\text{H}_2\text{O})]^{2+}$  as the catalysts at the irradiation of NIR.

As depicted in Fig. 5A, no NADPH was detected in the absence of r-GQDs, demonstrating that  $\text{TiO}_2$  semiconductor and the metal complex **M** alone were unable to induce light-generated electrons by NIR excitation (Fig. 5Aa). The yield of regenerated NADPH consistently increased throughout the illumination time and was significantly raised when 0.1 mM  $\text{NADP}^+$  was introduced, achieving 64 % after 90 min (Fig. 5Ab, Ac). Replacing the free mediator with the polymeric mediator,  $[\text{Cp}^*\text{Rh}(\text{bipy})\text{H}_2\text{O}]^{2+}$ , did not affect the reactivity of hydride transfer, as demonstrated by the similar rising trend observed in the corresponding cofactor regeneration curve and the good yield (67 %) at 75 min (Fig. 5Ad). Furthermore, the catalytic efficiencies of  $\text{TiO}_2/\text{r-GQDs}$  and cross-linked  $[\text{Cp}^*\text{Rh}(\text{bipy})\text{H}_2\text{O}]^{2+}$  were stable with a slight increase in yield observed

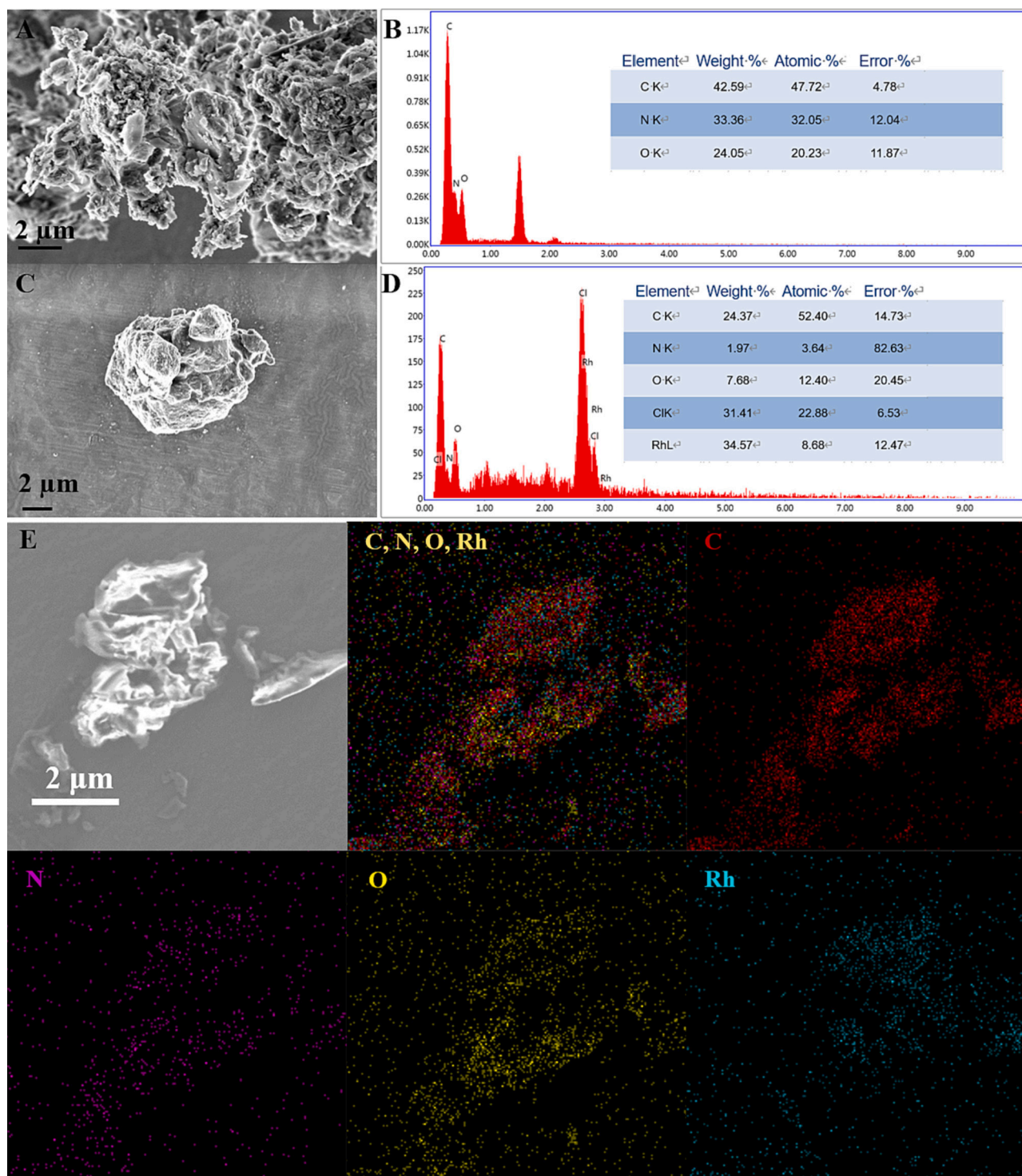


Fig. 3. SEM images of polymeric ligands (A) and M (C); EDS mapping of polymeric ligands (B) and M (D/E).

during the second cycle of cofactor regeneration under NIR-driven photocatalysis (Fig. 5Ae).

#### 3.4. Infrared light-catalysed synthesis of (*R*)-1-[3,5 bis(trifluoromethyl) benzene] ethanol

Microorganisms rely on cascades of reactions catalysed by mutually compatible and functionally specific enzymes to synthesize complex natural products and other metabolites. Not only does photobiosynthesis show that enzymes and photocatalysts are compatible, but also that the

combination can be productive. We used this approach to create important active pharmaceutical intermediates [56]. For example, (*R*)-1-[3,5-bis(trifluoromethyl)phenyl]ethanol [(*R*)-3,5-BTPE], a key intermediate for Aprepitant, a multifunctional antiemetic agent used to prevent postoperative or cancer chemotherapy-related nausea and vomiting [57–59]. Typical methods for (*R*)-3,5-BTPE synthesis with high enantioselectivity include chemical catalysis and enzymatic cascade transformation [60]. Chemical synthesis of (*R*)-3,5-BTPE is unsustainable for it depends on the enantioselectivity of (transitional) metal complexes containing complicated chiral ligands and harsh

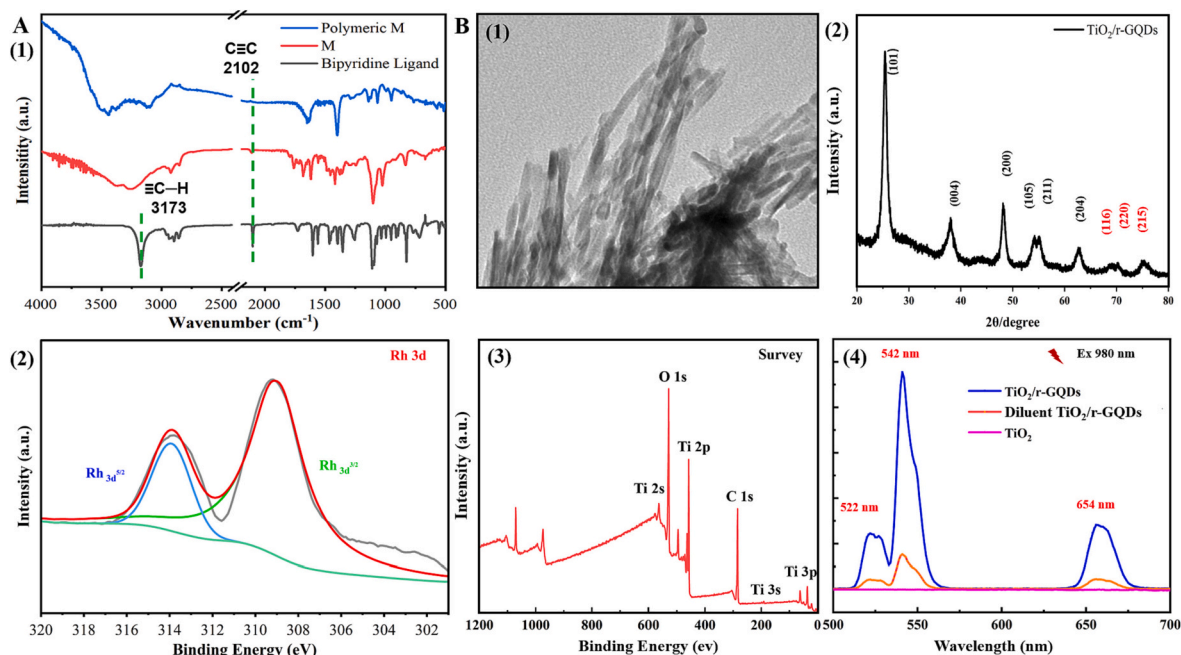


**Fig. 4.** A. (1) FT-IR spectra of polymeric **M**, **M** and the bipyridine ligand, (2) XPS spectra of Rh 3d for polymeric **M**; B. Characterization of  $\text{TiO}_2/\text{r-GQD}$  nanotubes: (1) SEM images, (2) XRD pattern, (3) XPS survey spectra, (4) Upconversion photoluminescence spectroscopy at 980 nm.

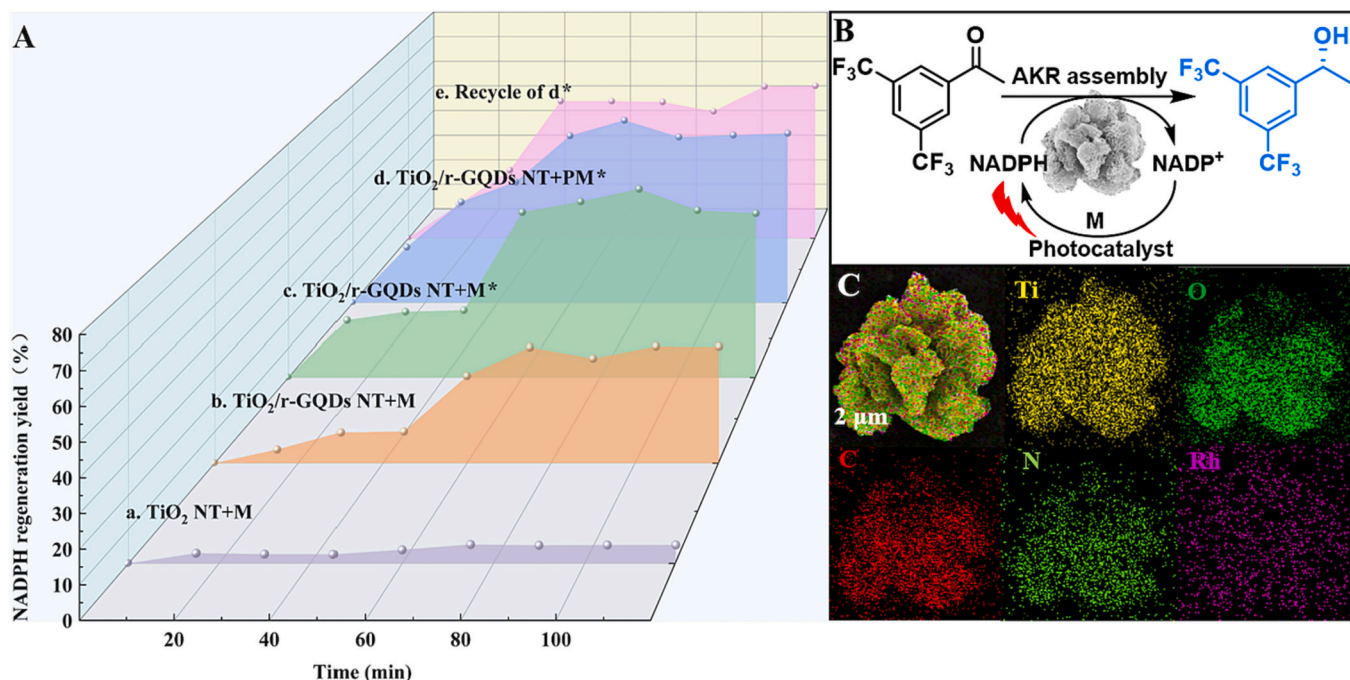


**Fig. 5.** (A) The regeneration yields of NADPH. Reaction conditions: PBS buffer (200 mM, 25 mL, pH 7.0),  $\text{TiO}_2/\text{r-GQDs}$  NT (20 mg),  $\text{NADP}^+$  (0.05 mM, 93 mg) and 0.25 mM **M** or polymeric **M** (**PM**), NIR irradiation. \*0.1 mM  $\text{NADP}^+$  was used. (B) Illustration of photo-enzymatic catalytic system with an SEM image of AKR-assembly- $\text{TiO}_2/\text{r-GQDs}$ -**M** hybrids. (C) EDS element mapping of AKR-assembly- $\text{TiO}_2/\text{r-GQDs}$ -**M** hybrids.

reaction conditions including high concentrations of  $\text{H}_2$  and strong bases [61,62]. The enzymic method consists of keto reductase for reducing the ketone substrate and dehydrogenase for regenerating NADPH. However, the enzyme activity of dehydrogenase is very limited, especially in the face of a high dosage of organic compounds (e.g. isopropanol, glucose) that function as electron donors. Resulting byproducts (e.g. acetone and glucuronic acid) also cause difficult product separation [63].

Having established a workable photocatalytic platform for NADPH regeneration, we concentrated on applying it in an AKR-mediated

photocatalytic reduction (Fig. 5B). The major components consisted of AKR protein assemblies,  $\text{TiO}_2/\text{r-GQDs}$  nanotubes and the rhodium mediator. As shown in the SEM image (Fig. 5B) the sample consists of a micron-scale artificial photobioreactor based on a flower-shaped enzyme surface that is covered with nanoscale photocatalysts. Fig. 5C presents the EDS element mapping for the reactor. The Rh from the electron mediator **M** is uniformly dispersed in the reaction medium. The distribution of Ti is relatively concentrated, which implies a closer spatial distance between the photosensitizer and biocatalyst that may

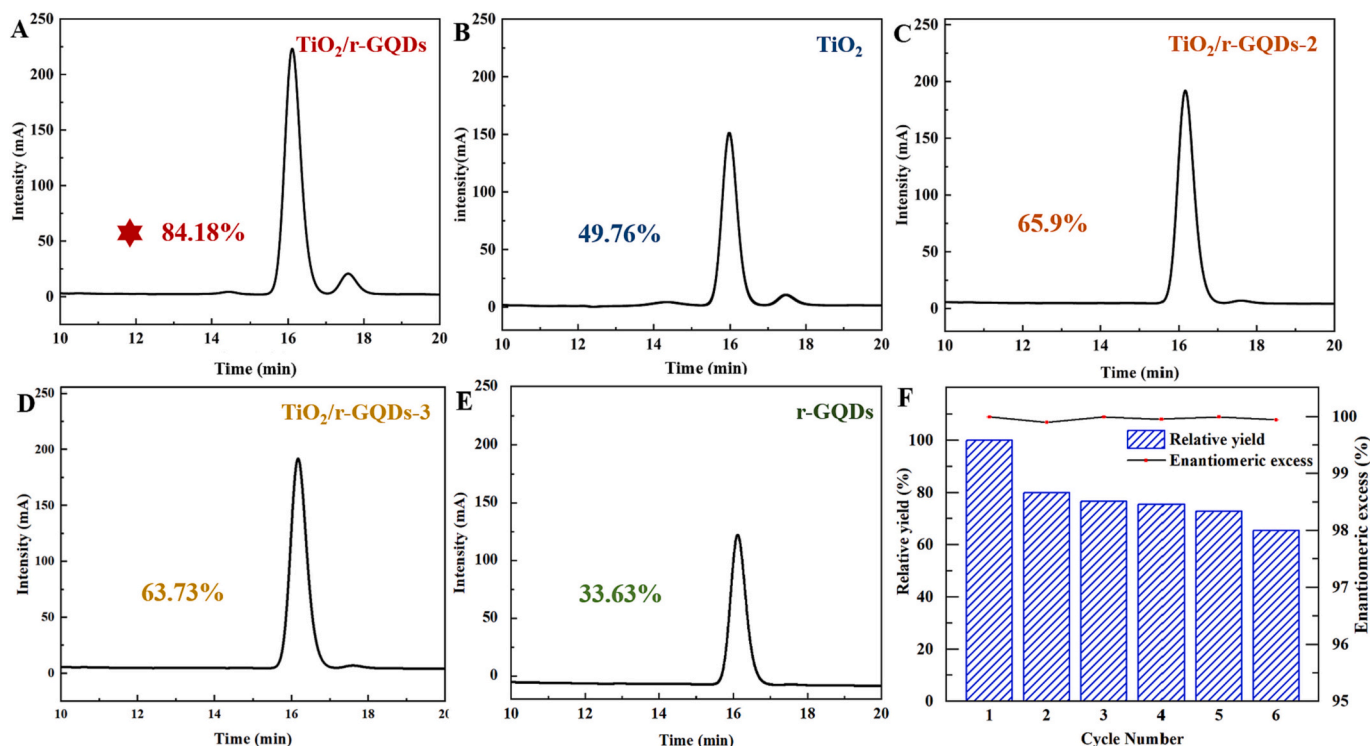


**Fig. 6.** The results of the photo-enzyme-catalysed reduction of 3,5-BTAP detected by reversed-phase HPLC: using  $\text{TiO}_2/\text{r-GQDs}$  (A),  $\text{TiO}_2$  (excitation wavelength  $\geq 420$  nm) (B),  $\text{TiO}_2/\text{r-GQDs-2}$  (C);  $\text{TiO}_2/\text{r-GQDs-3}$  (D); r-GQDs (E) as photocatalyst; (F) catalyst recycling.

result in a faster transfer rate of proton and cofactor.

The photobioreactor was used to hydrogenate 3,5-BTAP. Resulting (R)-3,5-BTPE was formed in 84 % yield with 99.98 % ee under NIR, thus verifying the high catalytic efficiency of this system (Fig. 6A). An additional control experiment shows that r-GQDs play a key role in the infrared light-induced catalytic reaction, during which the yield was just 50 % in the production of (R)-3,5-BTPE even using a strong energy illumination to irradiate  $\text{TiO}_2$  nanotubes photocatalyst for driving cofactor regeneration (Fig. 6B).

The relationship between  $\text{TiO}_2$  catalytic efficiency and the loading of r-GQDs was investigated under standard reaction conditions. When  $\text{TiO}_2/\text{r-GQDs-2}$  nano-composite, that had undergone two adsorptions of r-GQDs, was used the yield of (R)-3,5-BTPE decreased to 66 % (Fig. 6C). After three adsorptions of r-GQDs the yield of (R)-3,5-BTPE decreased further to 64 % (Fig. 6D). We speculated that excess coverage by r-GQDs would reduce the surface area available for electron transfer with other components like  $\text{H}_2\text{O}$  and the electron mediator. The yield under infrared light irradiation seriously declined to 34 % in the absence of  $\text{TiO}_2$  nanotubes (Fig. 6E). Thus, we conclude that the high performance of photobiocatalysis can be attributed to the combined effect of  $\text{TiO}_2$  nanotubes and r-GQDs.

To study the sustainability of our photo-enzymatic system, the recyclability of the AKR assembly,  $\text{TiO}_2/\text{r-GQDs}$  nano-composite and polymeric mediator was examined in the (R)-3,5-BTPE synthesis (Fig. S8). In general, the activity of the photo-enzyme components was stable except in the second cycle, and retains 66 % of its original catalytic efficiency after 6 cycles (Fig. 6F). However, the high enantioselectivity was maintained at 99.99 %, which further supports the biocompatibility of this NIR driven photo-enzymatic catalytic reaction (Fig. 6F).

#### 4. Conclusions

We have demonstrated the feasibility of facile, green and efficient NIR-driven photobiocatalysis using a novel combination of an AKR with

$\text{TiO}_2/\text{r-GQDs}$  hybrid nanotubes and a polymeric Rh electron mediator for NADPH regeneration in the production of the (R)-1-[3,5-bis(trifluoromethyl)phenyl]ethanol using water as the sacrificial reductant. The catalytic performance of photo-excited electron transfer in the  $\text{TiO}_2/\text{r-GQDs}$  system was investigated and the Ti-O-C linkage formed between r-GQDs and  $\text{TiO}_2$  was shown to play a vital role in photon upconversion under NIR irradiation. However, this study focuses on the recyclability of the entire photo-enzymatic system but less attention was paid to the distance between electron mediator and AKR, which would impact regenerated NADPH transfer and diffusion. In future studies, the preparation method will be optimized to achieve higher cofactor transfer efficiency.

#### CRediT authorship contribution statement

**Li Qiao:** Methodology, Investigation, Visualization, writing-reviewing and editing. **Jing Zhang:** Methodology, Writing the original draft. **Yongjian Jiang and Bianqin Ma:** Investigation, Formal analysis, Data curation. **Haomin Chen:** Formal analysis. **Peng Gao:** Validation, Methodology. **Pengfei Zhang:** Supervision, Validation. **Anming Wang:** Supervision, Conceptualization, Project administration, Funding acquisition, Conceptualization. **Roger A. Sheldon:** writing - reviewing & editing, Supervision.

#### Declaration of competing interest

The authors declare that they have no known competing financial interests or personal relationships that could have appeared to influence the work reported in this paper.

#### Data availability

Data will be made available on request.

## Acknowledgements

This study was supported by the National Natural Science Foundation of China (22078079, 22378091), the Natural Science Foundation of Zhejiang Province (LY18B060009), and the Program for Postgraduates in Innovation Practice and Service for Locality in HZNU (2022).

## Appendix A. Supplementary data

Supplementary data to this article can be found online at <https://doi.org/10.1016/j.ijbiomac.2024.130612>.

## References

- L. Qiao, Z. Luo, H. Chen, P. Zhang, A. Wang, R.A. Sheldon, Engineering ketoreductases for the enantioselective synthesis of chiral alcohols, *Chem. Commun.* 59 (2023) 7518–7533, <https://doi.org/10.1039/d3cc01474f>.
- R. Buller, S. Lutz, R.J. Kazlauskas, R. Snajdrova, J.C. Moore, U.T. Bornscheuer, From nature to industry: harnessing enzymes for biocatalysis, *Science* 382 (2023) eadh8615, <https://doi.org/10.1126/science.adh8615>.
- A.K. Gilio, T.W. Thorpe, N. Turner, G. Grogan, Reductive aminations by imine reductases: from milligrams to tons, *Chem. Sci.* 13 (2022) 4697–4713, <https://doi.org/10.1039/D2SC00124A>.
- A.I. Benítez-Mateos, D. Roura Padrosa, F. Paradisi, Multistep enzyme cascades as a route towards green and sustainable pharmaceutical syntheses, *Nat. Chem.* 14 (2022) 489–499, <https://doi.org/10.1038/s41557-022-00931-2>.
- J. Kim, Y. Um, S. Han, T. Hilberath, Y.H. Kim, F. Hollmann, C.B. Park, Unbiased photoelectrode interfaces for solar coupling of lignin oxidation with biocatalytic C=C bond hydrogenation, *ACS Appl. Mater. Interfaces* 14 (2022) 11465–11473, <https://doi.org/10.1021/acsami.1c24342>.
- V.K. Sharma, J.M. Hutchison, A.M. Allgeier, Redox biocatalysis: quantitative comparisons of nicotinamide cofactor regeneration methods, *ChemSusChem* 15 (2022) e202200888, <https://doi.org/10.1002/cssc.202200888>.
- J. Xu, Z. Ju, W. Zhang, Y. Pan, J. Zhu, J. Mao, X. Zheng, H. Fu, M. Yuan, H. Chen, R. Li, Efficient infrared-light-driven CO<sub>2</sub> reduction over ultrathin metallic ni-doped CoS<sub>2</sub> nanosheets, *Angew. Chem. Int. Ed.* 60 (2021) 8705–8709, <https://doi.org/10.1002/anie.202017041>.
- L. Huang, T. Le, K. Huang, G. Han, Enzymatic enhancing of triplet-triplet annihilation upconversion by breaking oxygen quenching for background-free biological sensing, *Nat. Commun.* 12 (2021) 1898, <https://doi.org/10.1038/s41467-021-22282-1>.
- S. Nishioka, F.E. Osterloh, X. Wang, T.E. Mallouk, K. Maeda, Photocatalytic water splitting, *Nat. Rev. Methods Prim.* 3 (2023) 42, <https://doi.org/10.1038/s43586-023-00226-x>.
- Z. Zhang, J. Tong, X. Meng, Y. Cai, S. Ma, F. Huo, J. Luo, B.-H. Xu, S. Zhang, M. Pinelo, Development of an ionic porphyrin-based platform as a biomimetic light-harvesting agent for high-performance photoenzymatic synthesis of methanol from CO<sub>2</sub>, *ACS Sustain. Chem. Eng.* 9 (2021) 11503–11511, <https://doi.org/10.1021/acscuschemeng.1c03737>.
- S.H. Lee, D.S. Choi, S.K. Kuk, C.B. Park, Photobiocatalysis: activating redox enzymes by direct or indirect transfer of photoinduced electrons, *Angew. Chem. Int. Ed.* 57 (2018) 7958–7985, <https://doi.org/10.1002/anie.201710070>.
- Y. Ashida, Y. Onozuka, K. Arashiba, A. Konomi, H. Tanaka, S. Kuriyama, Y. Yamazaki, K. Yoshizawa, Y. Nishibayashi, Catalytic nitrogen fixation using visible light energy, *Nat. Commun.* 13 (2022) 7263, <https://doi.org/10.1038/s41467-022-34984-1>.
- E.J. Son, Y.W. Lee, J.W. Ko, C.B. Park, Amorphous carbon nitride as a robust photocatalyst for biocatalytic solar-to-chemical conversion, *ACS Sustain. Chem. Eng.* 7 (2018) 2545–2552, <https://doi.org/10.1021/acscuschemeng.8b05487>.
- Y. Yin, R. Wang, J. Zhang, Z. Luo, Q. Xiao, T. Xie, X. Pei, P. Gao, A. Wang, Efficiently enantioselective hydrogenation photosynthesis of (R)-1-[3,5-Bis(trifluoromethyl)phenyl] ethanol over a CLEs-TiO<sub>2</sub> bioinorganic hybrid materials, *ACS Appl. Mater. Interfaces* 13 (2021) 41454–41463, <https://doi.org/10.1021/acsami.1c11050>.
- F. Lan, Q. Wang, H. Chen, Y. Chen, Y. Zhang, B. Huang, H. Liu, J. Liu, R. Li, Preparation of hydrophilic conjugated microporous polymers for efficient visible light-driven nicotinamide adenine dinucleotide regeneration and photobiocatalytic formaldehyde reduction, *ACS Catal.* 10 (2020) 12976–12986, <https://doi.org/10.1021/acscatal.0c03652>.
- H. Zhao, L. Wang, G. Liu, Y. Liu, S. Zhang, L. Wang, X. Zheng, L. Zhou, J. Gao, J. Shi, Y. Jiang, Hollow Rh-COF@COF S-scheme heterojunction for photo-catalytic nicotinamide cofactor regeneration, *ACS Catal.* 13 (2023) 6619–6629, <https://doi.org/10.1021/acscatal.2c06332>.
- Q. Feng, X. Zhou, C. He, NIR light-facilitated bone tissue engineering, *WIREs Nanomed. Nanobiotechnol.* n/a (2023) e1925, <https://doi.org/10.1002/wnan.1925>.
- R. Liu, Y. Peng, L. Lu, S. Peng, T. Chen, M. Zhan, Near-infrared light-triggered nano-prodrug for cancer gas therapy, *J. Nanobiotechnol.* 19 (2021) 443, <https://doi.org/10.1186/s12951-021-01078-x>.
- J. Feng, J. Alves, D.M. de Clercq, T.W. Schmidt, Photochemical upconversion, *Annu. Rev. Phys. Chem.* 74 (2023) 145–168, <https://doi.org/10.1146/annurev-physchem-092722-104952>.
- G. Lee, H.E. Choi, S.H. Hong, M. Choi, D.W. Han, J. Lee, K.S. Kim, S.K. Hahn, Upconversion nanomaterials and delivery systems for smart photonic medicines and healthcare devices, *Adv. Drug Deliv. Rev.* 188 (2022) 114419, <https://doi.org/10.1016/j.addr.2022.114419>.
- N. Xin, D. Wei, Y. Zhu, M. Yang, S. Ramakrishna, O. Lee, H. Luo, H. Fan, Upconversion nanomaterials: a platform for biosensing, theranostic and photo-regulation, *Mater. Today Chem.* 17 (2020) 100329, <https://doi.org/10.1016/j.mtchem.2020.100329>.
- B.S. Richards, D. Hudry, D. Busko, A. Turshatov, I.A. Howard, Photon upconversion for photovoltaics and photocatalysis: a critical review, *Chem. Rev.* 121 (2021) 9165–9195, <https://doi.org/10.1021/acs.chemrev.1c00034>.
- Z. Zhang, Y. Liu, Y. Fang, B. Cao, J. Huang, K. Liu, B. Dong, Near-infrared-plasmonic energy upconversion in a nonmetallic heterostructure for efficient H<sub>2</sub> evolution from ammonia borane, *Adv. Sci.* 5 (2018) 1800748, <https://doi.org/10.1002/advs.201800748>.
- M. Zhong, Z. Wang, D. Dai, B. Yang, S. Zuo, C. Yao, F. Wu, X. Li, Upconversion hollow nanospheres CeF<sub>3</sub> co-doped with Yb<sup>3+</sup> and Tm<sup>3+</sup> for photocatalytic nitrogen fixation, *J. Rare Earths* 40 (2022) 586–594, <https://doi.org/10.1016/j.jre.2021.03.004>.
- J. Liu, Y. Liu, N. Liu, Y. Han, X. Zhang, H. Huang, Y. Lifshitz, S.-T. Lee, J. Zhong, Z. Kang, Metal-free efficient photocatalyst for stable visible water splitting via a two-electron pathway, *Science* 347 (2015) 970–974, <https://doi.org/10.1126/science.aaa3145>.
- M. Levy, J.R. Bertram, K.A. Eller, A. Chatterjee, P. Nagpal, Near-infrared-light-triggered antimicrobial indium phosphide quantum dots, *Angew. Chem. Int. Ed.* 58 (2019) 11414–11418, <https://doi.org/10.1002/anie.201906501>.
- J. Li, H. Li, G. Zhan, L. Zhang, Solar water splitting and nitrogen fixation with layered bismuth oxyhalides, *Acc. Chem. Res.* 50 (2017) 112–121, <https://doi.org/10.1021/acs.accounts.6b00523>.
- J. Tian, Y. Leng, Z. Zhao, Y. Xia, Y. Sang, P. Hao, J. Zhan, M. Li, H. Liu, Carbon quantum dots/hydrogenated TiO<sub>2</sub> nanobelt heterostructures and their broad spectrum photocatalytic properties under UV, visible, and near-infrared irradiation, *Nano Energy* 11 (2015) 419–427, <https://doi.org/10.1016/j.nanoen.2014.10.025>.
- S.L. Wang, Y. Zhu, X. Luo, Y. Huang, J. Chai, T.I. Wong, G.Q. Xu, 2D WC/WO<sub>3</sub> heterogeneous hybrid for photocatalytic decomposition of organic compounds with Vis–NIR light, *Adv. Funct. Mater.* 28 (2018) 1705357, <https://doi.org/10.1002/adfm.201705357>.
- L. Huang, W. Wu, Y. Li, K. Huang, L. Zeng, W. Lin, G. Han, Highly effective near-infrared activating triplet-triplet annihilation upconversion for photoredox catalysis, *J. Am. Chem. Soc.* 142 (2020) 18460–18470, <https://doi.org/10.1021/jacs.0c06976>.
- O. Verho, J.-E. Bäckvall, Chemoenzymatic dynamic kinetic resolution: a powerful tool for the preparation of enantiomerically pure alcohols and amines, *J. Am. Chem. Soc.* 137 (2015) 3996–4009, <https://doi.org/10.1021/jacs.5b01031>.
- Y. Wang, H. Ren, H. Zhao, Expanding the boundary of biocatalysis: design and optimization of in vitro tandem catalytic reactions for biochemical production, *Crit. Rev. Biochem. Mol. Biol.* 53 (2018) 115–129, <https://doi.org/10.1080/10409238.2018.1431201>.
- C.A. Denard, H. Huang, M.J. Bartlett, L. Lu, Y. Tan, H. Zhao, J.F. Hartwig, Cooperative tandem catalysis by an organometallic complex and a metallo-enzyme, *Angew. Chem. Int. Ed.* 53 (2014) 465–469, <https://doi.org/10.1002/anie.201305778>.
- J.S. Lee, D.H. Nam, S.K. Kuk, C.B. Park, Near-infrared-light-driven artificial photosynthesis by nanobiocatalytic assemblies, *Chem. Eur. J.* 20 (2014) 3584–3588, <https://doi.org/10.1002/chem.201400136>.
- J. Wu, Y. Song, B. Han, J. Wei, Z. Wei, Y. Yang, Synthesis and characterization of UV upconversion material Y<sub>2</sub>SiO<sub>5</sub>:Pr<sup>3+</sup>, Li<sup>+</sup>/TiO<sub>2</sub> with enhanced the photocatalytic properties under a xenon lamp, *RSC Adv.* 5 (2015) 49356–49362, <https://doi.org/10.1039/c5ra06416c>.
- R. Lu, S.Z. Zhao, Y. Yang, Y. Wang, H.L. Huang, Y.D. Hu, R.D. Rodriguez, J.J. Chen, Efficient adsorption and photocatalytic degradation of organic contaminants using TiO<sub>2</sub>/(Bi<sub>2</sub>O<sub>3</sub>/Bi<sub>2</sub>O<sub>2.33</sub>) nanotubes, *Materials Today Chemistry* 32 (2023) 101641, <https://doi.org/10.1016/j.mtchem.2023.101641>.
- J. Wang, J. Jiang, F. Li, J. Zou, K. Xiang, H. Wang, Y. Li, X. Li, Emerging carbon-based quantum dots for sustainable photocatalysis, *Green Chem.* 25 (2023) 32–58, <https://doi.org/10.1039/D2GC03160D>.
- D. Jia, X. Li, Q. Chi, J. Low, P. Deng, W. Wu, Y. Wang, K. Zhu, W. Li, M. Xu, X. Xu, G. Jia, W. Ye, P. Gao, Y. Xiong, Direct electron transfer from upconversion graphene quantum dots to TiO<sub>2</sub> enabling infrared light-driven overall water splitting, *Research* 2022 (2022), <https://doi.org/10.34133/2022/9781453>.
- J.-i. Fujisawa, S. Matsumura, M. Hanaya, A single Ti-O-C linkage induces interfacial charge-transfer transitions between TiO<sub>2</sub> and a  $\pi$ -conjugated molecule, *Chem. Phys. Lett.* 657 (2016) 172–176, <https://doi.org/10.1016/j.cplett.2016.05.049>.
- X. Pei, Z. Luo, L. Qiao, Q. Xiao, P. Zhang, A. Wang, R.A. Sheldon, Putting precision and elegance in enzyme immobilisation with bio-orthogonal chemistry, *Chem. Soc. Rev.* 51 (2022) 7281–7304, <https://doi.org/10.1039/d1cs01004b>.
- T. Himiyama, M. Waki, Y. Maegawa, S. Inagaki, Cooperative catalysis of an alcohol dehydrogenase and rhodium-modified periodic mesoporous organo-silica, *Angew. Chem. Int. Ed.* 58 (2019) 9150–9154, <https://doi.org/10.1002/anie.201904116>.
- Y. Zhang, B. Wei, H. Liang, Rhodium-based MOF-on-MOF difunctional core-shell nanostructure for NAD(P)H regeneration and enzyme directed immobilization, *ACS Appl. Mater. Interfaces* 15 (2023) 3442–3454, <https://doi.org/10.1021/acsami.2c18440>.

- [43] R. Wang, J. Zhang, Z. Luo, T. Xie, Q. Xiao, X. Pei, A. Wang, Controllably crosslinked dual enzymes enabled by genetic-encoded non-standard amino acid for efficiently enantioselective hydrogenation, *Int. J. Biol. Macromol.* 205 (2022) 682–691, <https://doi.org/10.1016/j.ijbiomac.2022.02.171>.
- [44] H. Li, R. Wang, A. Wang, J. Zhang, Y. Yin, X. Pei, P. Zhang, Rapidly and precisely cross-linked enzymes using bio-orthogonal chemistry from cell lysate for the synthesis of (S)-1-(2,6-dichloro-3-fluorophenyl) ethanol, *ACS Sustain. Chem. Eng.* 8 (2020) 6466–6478, <https://doi.org/10.1021/acssuschemeng.0c00987>.
- [45] L. Qiao, Z. Luo, R. Wang, X. Pei, S. Wu, H. Chen, T. Xie, R.A. Sheldon, A. Wang, Designing an enzyme assembly line for green cascade processes using bio-orthogonal chemistry, *Green Chem.* 25 (2023) 7547–7555, <https://doi.org/10.1039/d3gc01898a>.
- [46] J. Zhang, R. Wang, Z. Luo, D. Jia, H. Chen, Q. Xiao, P. Zhang, X. Pei, A. Wang, Controlled chemical assembly of enzymes in cell lysate enabled by genetic-encoded nonstandard amino acids, *Mater. Chem. Front.* 6 (2022) 182–193, <https://doi.org/10.1039/d1qm01285a>.
- [47] J. Ryu, D.H. Nam, S.H. Lee, C.B. Park, Biocatalytic photosynthesis with water as an electron donor, *Chem. Eur. J.* 20 (2014) 12020–12025, <https://doi.org/10.1002/chem.201403301>.
- [48] T. Liu, B. Xiao, F. Xiang, J. Tan, Z. Chen, X. Zhang, C. Wu, Z. Mao, G. Luo, X. Chen, J. Deng, Ultrasmall copper-based nanoparticles for reactive oxygen species scavenging and alleviation of inflammation related diseases, *Nat. Commun.* (2020) 11, <https://doi.org/10.1038/s41467-020-16544-7>.
- [49] S. Mandal, R. Das, P. Gupta, B. Mukhopadhyay, Synthesis of a sugar-functionalized iridium complex and its application as a fluorescent lectin sensor, *Tetrahedron Lett.* 53 (2012) 3915–3918, <https://doi.org/10.1016/j.tetlet.2012.05.075>.
- [50] R. Wienkamp, E. Steckhan, Selective generation of NADH by visible light, *Angew. Chem. Int. Ed.* 22 (1983) 497, <https://doi.org/10.1002/anie.198304971>.
- [51] W. Jones, J.W.H. Burnett, J. Shi, R.F. Howe, X. Wang, Improving photocatalytic energy conversion via NAD(P)H, *Joule* 4 (2020) 2055–2059, <https://doi.org/10.1016/j.joule.2020.07.024>.
- [52] G. Lin, Y. Zhang, Y. Hua, C. Zhang, C. Jia, D. Ju, C. Yu, P. Li, J. Liu, Bioinspired metalation of the metal-organic framework MIL-125-NH(2) for photocatalytic NADH regeneration and gas-liquid-solid three-phase enzymatic CO<sub>2</sub> reduction, *Angew. Chem. Int. Ed.* 61 (2022) e202206283, <https://doi.org/10.1002/anie.202206283>.
- [53] Y. Cheng, J. Shi, Y. Wu, X. Wang, Y. Sun, Z. Cai, Y. Chen, Z. Jiang, Intensifying electron utilization by surface-anchored Rh complex for enhanced nicotinamide cofactor regeneration and photoenzymatic CO(2) reduction, *Research (Wash. D.C.)* 2021 (2021) 8175709, <https://doi.org/10.34133/2021/8175709>.
- [54] D. Khamboonrueang, S. Srirattanapibul, I.-M. Tang, S. Thongmee, TiO<sub>2</sub>• rGO nanocomposite as a photocatalyst for the reduction of Cr<sup>6+</sup>, *Mater. Res. Bull.* 107 (2018) 236–241, <https://doi.org/10.1016/j.materresbull.2018.07.002>.
- [55] O.S. Dahham, R. Hamzah, M.A. Bakar, N.N. Zulkepli, S.S. Ting, M.F. Omar, T. Adam, K. Muhamad, S.S. Dahham, Synthesis and structural studies of an epoxidized natural rubber/titania (ENR-50/TiO<sub>2</sub>) hybrid under mild acid conditions, *Polym. Test.* 65 (2018) 10–20, <https://doi.org/10.1016/j.polymertesting.2017.11.005>.
- [56] Z.C. Litman, Y.J. Wang, H.M. Zhao, J.F. Hartwig, Cooperative asymmetric reactions combining photocatalysis and enzymatic catalysis, *Nature* 560 (2018) 355–359, <https://doi.org/10.1038/s41586-018-0413-7>.
- [57] P. Rodriguez-Jimenez, P. Chicharro, M. Llamas-Velasco, B. Moyano, I. Sanchez-Carpintero, J.C. Lopez-Gutierrez, V. Martinez-Glez, L. Rodriguez-Laguna, A. Torreló, A case of naevus vascularis mixtus with hypotrophy and hypotrichosis due to mosaic GNA11 mutation, *J. Eur. Acad. Dermatol. Venereol.* 34 (2020) e420–e422, <https://doi.org/10.1111/jdv.16369>.
- [58] V. Noronha, A. Bhattacharjee, V.M. Patil, A. Joshi, N. Menon, S. Shah, S. Kannan, S. A. Mukadam, K. Maske, S. Ishi, K. Prabhash, Aprepitant for cough suppression in advanced lung cancer, *Chest* 157 (2020) 1647–1655, <https://doi.org/10.1016/j.chest.2019.11.048>.
- [59] H. D'Souza, V. Noronha, V.M. Patil, A. Joshi, N.S. Menon, K. Prabhash, Aprepitant in weekly cisplatin with radiation in head and neck cancer: is it required? *J. Clin. Oncol.* 38 (2020) e24122, [https://doi.org/10.1200/JCO.2020.38.15\\_suppl.e24122](https://doi.org/10.1200/JCO.2020.38.15_suppl.e24122).
- [60] Z. Duan, Y. Wang, B. Ouyang, P. Wang, Efficient asymmetric synthesis of ethyl (R)-3-hydroxybutyrate by recombinant *Escherichia coli* cells under high substrate loading using eco-friendly ionic liquids as cosolvent, *Bioprocess Biosyst. Eng.* 46 (2023) 1293–1302, <https://doi.org/10.1007/s00449-023-02897-y>.
- [61] W. Wu, N. Zhao, Y. Liu, S. Du, X. Wang, W. Mo, X. Yan, C. Xu, Y. Zhou, B. Ji, Iridium catalysts with *f*-amphibinol ligands: highly stereoselective hydrogenation of a variety of ketones, *Org. Lett.* 25 (2023) 8845–8849, <https://doi.org/10.1021/acscorglett.3c03550>.
- [62] R. Bigler, R. Huber, M. Stöckli, A. Mezzetti, Iron(II)/(NH)<sub>2</sub>P<sub>2</sub> macrocycles: modular, highly enantioselective transfer hydrogenation catalysts, *ACS Catal.* 6 (2016) 6455–6464, <https://doi.org/10.1021/acscatal.6b01872>.
- [63] X. Wang, T. Saba, H.H.P. Yiu, R.F. Howe, J.A. Anderson, J. Shi, Cofactor NAD(P)H regeneration inspired by heterogeneous pathways, *Chem* 2 (2017) 621–654, <https://doi.org/10.1016/j.chempr.2017.04.009>.